JOURNAL OF MATERIALS SCIENCE 23 (1988) 1943–1947

Effect of temperature on the oxidation of Fe–7.5Al–0.65C alloy

C. H. KAO, C. M. WAN
Institute of Materials Science and Engineering, National Tsing Hua University, Hsinchu, Taiwan

An alloy with the chemical composition Fe–7.5Al–0.65C was employed to investigate the effect of temperature on oxidation between 600 and 900° C in dry air. Kinetic curves were determined by thermogravimetry analyses (TGA). Optical metallography and electron probe microanalysis (EPMA) were used to examine the oxide scales. At 600° C, the initial stage of oxidation followed a parabolic rate law, and oxidation subsequently, increased dramatically. Internal oxidation occurred beneath the nodule formed on the present alloy at 600° C. In contrast, no internal oxidation could be found in specimens of the Fe–7.5Al–0.65C alloy after oxidizing at 700, 800 and 900° C. The kinetic results have two distinct parabolic rates for the present alloy.

1. Introduction

A number of investigators [1–6] have reported the oxidation behaviour of alloys based on iron and aluminium. The Fe–Al alloys have long been recognized to have excellent high-temperature oxidation resistance due to the formation of a protective α-Al_2O_3 layer during the oxidation process. However, few data are available on the effect of carbon on the oxidation resistance of Fe–Al alloys, and results of the investigations on other steels and alloys have been contradictory.

Boggs and Kachik [7] found that Fe–C oxidized faster than iron at 500° C, possibly because the Fe_3C in the substrate suppressed the formation of oxide blisters. Caplan *et al.* [8] found that the oxidation rate of Fe–0.5 wt % C and Fe–1.0 wt % C alloys was slower than that of pure iron at 1 atm O_2 and 700° C. A residue of graphite was identified at the metal–oxide interface, suggesting that this film hindered the transfer of metal to the oxide, thus slowing the oxidation rate. Similar studies by Malik and Whittle [9] in the temperature range 600 to 850° C also indicated that the oxidation rate of Fe–C alloys was slower than that of pure iron. However, there was no real evidence of carburization of the alloy at the alloy–scale interface. They suggested that the presence of carbon lowered the oxidation rate relative to that of pure iron and this had been related to the rejection of carbon at the alloy–scale interface, causing poor contact between scale and alloy.

Abderrazik *et al.* [10] indicated that carbon had a strong influence on alumina growth and adherence of Fe–23Cr–5Al alloy. Competition between oxidation and carbide precipitation slightly increases the oxidation rate during isothermal treatments but has a beneficial influence on the oxide scale adherence. Ryl'nikov *et al.* [11] found that the beneficial effect of carbon on the scaling resistance of iron–aluminium-based alloys involves its influence on the thermal stability of the K-phase. The higher the carbon content of the alloy, the higher is its content in the K-phase, stabilizing it and giving it more resistance to dissolution at high temperature.

Our previous work [12] with Fe–5.5Al–0.55C at 600, 800 and 1000° C showed that temperature strongly influenced the stability of the K-phase. The amount of dissociation of K-phase in the matrix increased with increasing temperature, which resulted in different kinetic behaviour during the oxidation process. The purpose of the present work was to carry out a series of oxidation experiments with Fe–7.5Al–0.65C alloy with the aim of understanding the oxidation behaviour of Fe–Al–C alloy.

2. Experimental procedure

The chemical composition of the alloy used for the present study is shown in Table I. The alloy was prepared with an air induction furnace under a controlled protective argon atmosphere. The cast ingot was hot forged at 1200° C from 7 cm down to 2.5 cm and then homogenized at 1100° C for 4 h. After surface finishing, the surface and edges of the specimens were mechanically polished with abrasive paper up to 1200 grit. Each specimen was finally cleaned ultrasonically in acetone before the oxidation experiment was performed.

The kinetics of oxidation were performed in the infrared image furnace of an ULVAC/SHINKURIKO thermobalance in dry air with a flow rate of 100 ml min^{-1}. The oxidation period was 24 h and the heating and cooling rate of the infrared image furnace was 100° C min^{-1}. The temperatures used in the experiment ranged from 600 to 900° C and were

TABLE I Chemical composition (wt %) of the alloy tested

Al	C	Mn	Si	P	S	Fe
7.54	0.65	0.01	0.015	0.01	0.01	Bal.

0022–2461/88 $03.00 + .12

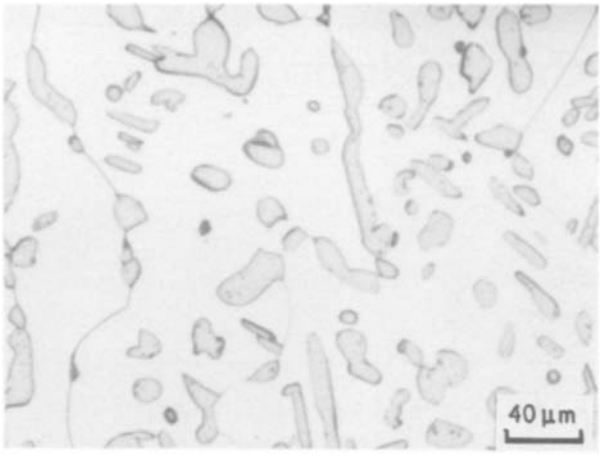

Figure 1 Fe–7.5Al–0.65C microstructure after heat treatment (4 h at 1100° C).

increased in increments of 100° C. The specimen temperature and weight-gain curves of oxidation were recorded using a chart recorder.

The possible phases present in the diffraction specimens were identified using X-ray diffraction with a copper target, nickel filter and a graphite single-crystal monochrometer. The morphology of the oxide scale was examined by optical microscopy. The elemental redistribution and concentration profile in the oxidized specimens were characterized by an electron microprobe, EPMA (Jeol, JCXA-733). The quantitative analysis of iron and aluminium was performed with the aid of a ZAF-corrected program. EPMA operation was carried out by first accelerating the voltage to 25 kV with a probe current of 0.03 μA.

3. Results and discussion

Fig. 1 shows the microstructure of Fe–7.5Al–0.65C alloy after hot forging at 1200° C and 4 h homogenization at 1100° C. A two-phase material with iron–aluminium carbide (Fe_3AlC_x) was found in the ferrite matrix using X-ray diffraction. The dark areas in the micrograph are iron–aluminium carbide particles (Fe_3AlC_x), whereas light areas are the ferrite regions. The lattice parameters were 0.287 and 0.378 nm for ferrite and carbide, respectively.

Fig. 2 shows the kinetic curves of oxidation of the Fe–7.5Al–0.65C alloy with different experimental temperatures. The figure indicates that the oxidation rate did not increase on increasing the temperature from 600 to 900° C. It was also observed that the weight gain of the alloy oxidation at 700° C increased rapidly during the initial oxidation period, then a steady state of oxidation followed, possibly through the formation of a healing layer beneath the growing oxide. The oxidation–time curves for Fe–7.5Al–0.65C alloy also show that the points at 800 and 900° C fall below those for 600 and 700° C after 24 h oxidation. It appears that in all cases, except at 600° C, the oxidation rate gradually decreased with time and finally approached a plateau after a longer exposure time. The kinetic results at 700, 800 and 900° C showed two distinct parabolic rates for the present alloy.

TABLE II Parabolic rate constants for the oxidation of Fe–7.5Al–0.65C alloy at 600 to 900° C

Temperature (° C)	K_{p1} ($g^2\,cm^{-4}\,sec^{-1}$)	K_{p2} ($g^2\,cm^{-4}\,sec^{-1}$)
600	2.4×10^{-12} (< 4 h)	–
700	6.4×10^{-11} (< 4 h)	2.2×10^{-12} (> 14 h)
800	4.9×10^{-12} (< 4 h)	0.6×10^{-12} (> 12 h)
900	5.6×10^{-12} (< 4 h)	1.0×10^{-13} (> 10 h)

It is very interesting to note that the oxidation rate of the alloy does not obey the simple parabolic rate and two distinct parabolic rate laws at 600° C within 24 h, as shown in Fig. 2. According to the square of weight gain–time curve, the initial stage of oxidation follows a parabolic rate law, then a decrease in the oxidation resistance was observed which does not obey the same law. The calculated value of the parabolic constant (K_{p1}) is 2.4×10^{-10} $g^2\,cm^{-4}\,sec^{-1}$. All the parabolic rate constants were calculated and are listed in Table II. The initial parabolic rate constant (K_{p1}) of the present alloy increased with increasing oxidation temperature at 700 to 900° C. In contrast, the final parabolic rate constant (K_{p2}) decreased on increasing the temperature from 700 to 900° C.

The oxide layers formed on the surface of the Fe–7.5Al–0.65C alloy after 24 and 96 h oxidation at 600° C are shown in Figs 3 and 4, respectively. No decarburization could be observed in these conditions. It was observed that nodules formed on the surface of the Fe–7.5Al–0.65C alloy and an internal oxidation

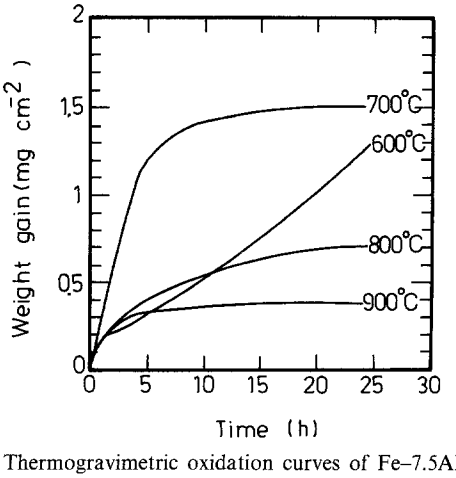

Figure 2 Thermogravimetric oxidation curves of Fe–7.5Al–0.65C alloy at different temperatures.

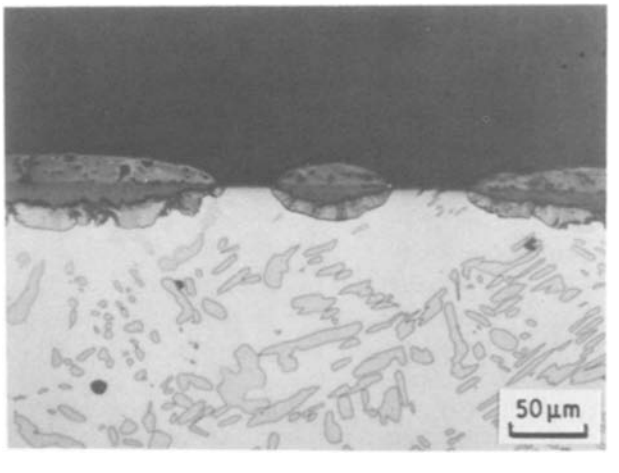

Figure 3 Metallographic cross-section of the nodules on Fe–7.5Al–0.65C alloy after 24 h oxidation at 600° C.

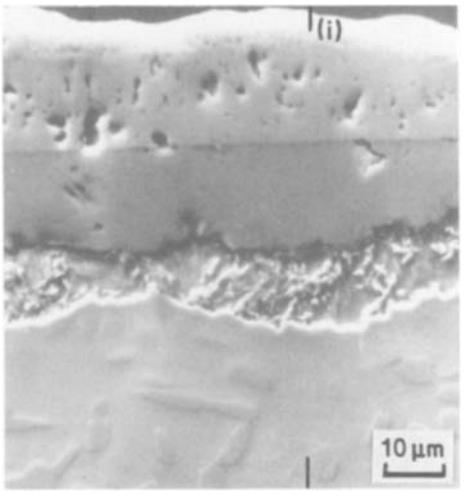

Figure 4 Scanning electron micrograph of the oxide on Fe–7.5Al–0.65C alloy after 96 h oxidation at 600° C.

TABLE III Electron microprobe point analysis of oxide layers on Fe–7.5Al–0.58C after 6, 12, 24, 48 and 96 h at 600° C

Oxidation time (h)	Layer	Fe(wt %)	Al(wt %)
6	inner	70.9–73.8	9.6–12.7
	middle	50.9–57.2	12.2–15
	outer	65–65.6	0
12	inner	72.8–79	10.5–17.8
	middle	49.9–54.4	9.7–16
	outer	61–67.4	0
24	inner	82.75	17.65
	middle	49.7–54	13.8–15.8
	outer	62.8–68.4	0
48	inner	81.9–82.3	10–13
	middle	50.2–53.3	12.9–14.7
	outer	64.9–67.5	0
96	inner	73.8–83.4	9.0–11.4
	middle	54	12–14.5
	outer	61.2–67.2	0

product existed beneath the nodules. The concentration of elements in these layers and in the matrix of the alloy oxidized for 96 h at 600° C, determined by electron microprobe using a line scanning profile technique, is shown in Fig. 5. Table III summarizes the quantitative results of aluminium and iron contents, obtained by electron microprobe point analysis. Through EPMA and X-ray diffraction investigations, the outer, middle and inner layers were found to be Fe_2O_3, $(Fe_xAl_{1-x})_2O_3$ and an internal oxide of aluminium, respectively. Fig. 6 shows an optical micrograph of the cross-section of Fe–7.5Al–0.65C alloy after 24 h at 700° C and many nodules could be observed. No internal oxide and no decarburization could be observed under these conditions. From the results of line profile and X-ray mapping of EPMA, there is an outer porous layer of uniform iron content and an inner layer that is enriched with aluminium. The metallographic appearance from the cross-sectional area of the 24 h oxidized alloy at an oxidation temperature of 800° C indicated the existence of a few small nodules and Al_2O_3 on the surface. In contrast, no nodules were observed on the surface of the alloy oxidized for 24 h at a temperature of 900° C. Fig. 7 shows a metallographic cross-section of the oxide scale present on the alloy after 24 h at 900° C. No decarburization could be observed under these conditions. This is in agreement with the oxidation kinetics: the final weight gain of this alloy at 900° C is the lowest among the different experimental temperatures from 600 to 900° C, as shown in Fig. 2.

An important question is: why does internal oxidation occur beneath the nodules formed on Fe–7.5Al–0.65C alloy at 600° C, but not occur at 700° C and above? At 600° C, nodules containing Fe_2O_3 and $(FeAl)_2O_3$ were observed, while a significant degree of internal oxidation was also seen. No carbide-free layer could be observed in the alloy under such conditions. All these facts suggested that carbide was quite stable in the matrix of the alloy during the oxidation experiment at 600° C. It seems that the effect of carbon on the oxidation behaviour of the alloy is only closely correlated with the decomposition along the oxide–matrix interface under such conditions. According to the results obtained from optical morphology, EPMA and the X-ray diffraction investigations the formation of nodules and the internal oxidation formation mechanism of the present alloy at 600° C are thought to occur as follows. The initial stage of oxidation is characterized by the formation of nuclei of Al_2O_3, FeO and CO (or CO_2), then CO (or CO_2) evaporates in to

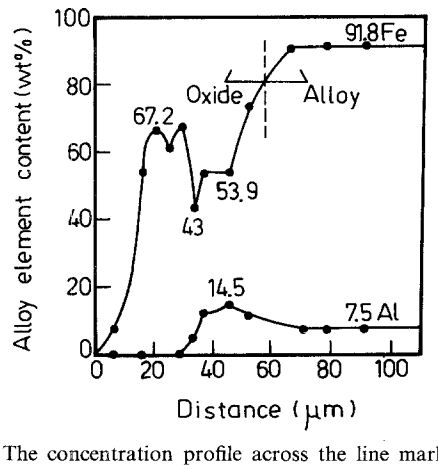

Figure 5 The concentration profile across the line marked (i) in Fig. 4.

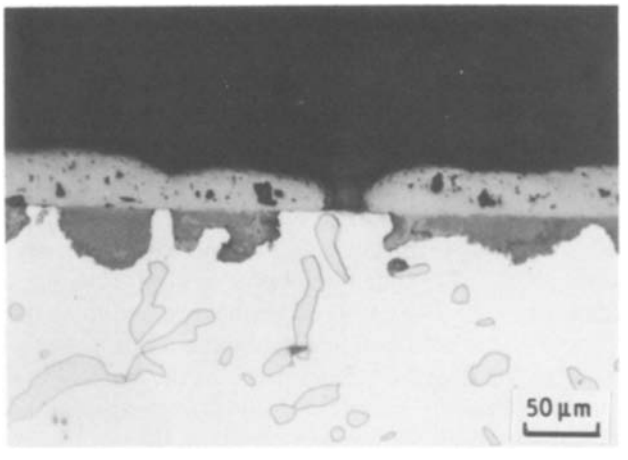

Figure 6 Metallographic cross-section of the nodules on Fe–7.5Al–0.65C alloy after 24 h oxidation at 700° C.

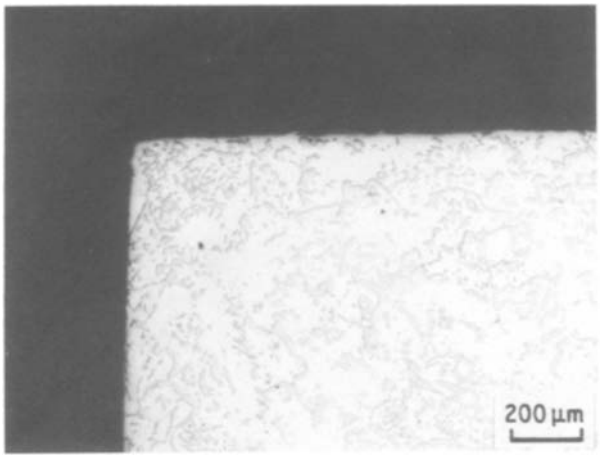

Figure 7 Metallographic cross-section of the oxide on Fe–7.5Al–0.65C alloy after 24 h oxidation at 900° C.

the environment from the surface of specimen. The concentration of aluminium is sufficient for Al_2O_3 grains to cover the alloy surface and FeO remains at randomly located sites. As the oxidation time is increased, the outer surface of FeO further reacts to form higher oxide nodules. Generally, CO (or CO_2) gas transports through the scales via pores and microcracks, which supports rapid diffusion channels for oxygen from the environment to the alloy. As oxidation proceeds, more oxygen can diffuse through the iron oxide of the nodule into the substrate, where it then reacts with aluminium to form the dispersed alumina phase. The internal oxidation process prevents the diffusion of aluminium to the nodule–alloy interface. This would explain why the kinetics of the Fe–7.5Al–0.65C alloy oxidized at 600° C do not obey the simple parabolic rate law and two distinct parabolic rate laws.

Several authors [13–17] reported that internal oxidation occurred when irons containing silicon, aluminium or manganese are oxidized. There are several interrelated factors of importance in determining whether the oxide of the solute metal will precipitate internally or form as a continuous layer on the surface. The solute concentration is not the only factor of importance. Wagner [18] proposed that if the volume fraction of the oxide of the alloying element reaches a critical value, the diffusion paths for oxygen into the alloy become important.

At 700 and 800° C, oxide scales with some nodules were formed on the Fe–7.5Al–0.65C alloy and no internal oxidation could be observed. It was also found that the number of nodules decreased with increasing temperature. Fig. 7 shows that no nodules or internal oxidation could be found on the alloy oxidized for 24 h at 900° C. This can be taken as an indication that the oxidation rate of the alloy oxidized at 700° C is higher than that of alloys oxidized at 800 and 900° C. The final weight gain of the oxidized specimen after 24 h at 700° C mainly resulted from the formation of such nodules. A similar result was also reported by Boggs and Kachik [7]. As the temperature increased, and the mobility of aluminium atoms in the metal increased, more and more of the protective aluminium oxide was formed, fewer and fewer iron nodules, and the overall oxidation rate dropped. The mechanism for nodule formation on the alloy at 700° C is similar to that described previously. However, internal oxidation ahead of a growing nodule can be suppressed by the formation of a healing layer of Al_2O_3 or $FeAl_2O_4$ which act as barriers to the outward diffusion of iron cations. At 800° C, growth of nodules was rapidly suppressed and their size was correspondingly small. Nodule growth was not observed on the surface of the alloy after 24 h oxidation at 900° C. The decomposition of the carbide along the oxide–matrix interface in the initial stage becomes ineffective. It appears that under these conditions the flux of aluminium in the alloy is sufficient to ensure the stability of a spinel layer or alumina oxide scale on the alloy, which resulted in the reduction of oxygen activity and, consequently, the inhibition of internal oxidation of aluminium.

According to the previous interpretation, the change in the oxidation behaviour observed between 600 and 700 to 900° C is related to the effect of temperature on the diffusion of aluminium in the alloy.

4. Conclusions

1. The oxidation behaviour of the Fe–7.5Al–0.65C alloy oxidized for 24 h at 600 to 900° C can be classified into two types. The change in the oxidation behaviour observed between 600 and 700 to 900° C is related to the effect of temperature on the diffusion of aluminium in the alloy.

2. During oxidation of the alloy at 600° C, the initial stage of oxidation follows a parabolic rate law, and then a subsequent decrease in the oxidation resistance was observed which does not obey a simple parabolic rate law. Internal oxidation occurred beneath the nodules formed on Fe–7.5Al–0.65C alloy under these conditions.

3. No internal oxidation could be observed in specimens of the Fe–7.5Al–0.65C alloy after 24 h oxidation at 700, 800 and 900° C. The kinetic results showed two distinct parabolic rates for the present alloy.

4. The transition temperature from internal to external oxidation was found to be between 600 and 700° C.

Acknowledgement

The authors acknowledge the financial support of this research by the National Science Council, Republic of China, under Grant NSC75-0201-E007-03.

References

1. F. SAEGUSA and L. LEE, *Corrosion* **22** (1966) 168.
2. W. E. BOGGS, *J. Electrochem. Soc.* **118** (1971) 906.
3. E. R. MORGAN and V. F. ZACKAY, *Metal Progr.* October (1955) 126.
4. P. TOMASEWICA and G. R. WALLWORK, *Oxid. Metals* **19** (1983) 165.
5. W. E. HAGEL, *Corrosion* **12** (1956) 316.
6. T. NAKAYAMA and K. KANEKO, *ibid.* **26** (1970) 187.
7. W. E. BOGGS and R. H. KACHIK, *J. Electrochem. Soc.* **116** (1969) 424.
8. O. CAPLAN *et al.*, *Oxid. Metals* **13** (1979) 255.
9. A. U. MALIK and D. P. WHITTLE, *ibid.* **16** (1981) 339.
10. G. BEN ABDERRAZIKM, G. MOULIN and A. M. HUNTZ, *J. Mater. Sci.* **19** (1984) 3173.

11. B. S. RYL'NIKOV *et al.*, *Zashchita Metallov* **19** (1983) 983.
12. C. H. KAO and C. M. WAN, *J. Mater. Sci.* **22** (1987) 3203.
13. J. H. SWISHER and E. T. TURKDOGAN, *Trans. TMS-AIME* **239** (1967) 426.
14. J. L. MEIJERING, *Acta Metall.* **3** (1955) 157.
15. H. BOHNENKAMP and H. J. ENGELL, *Arch. Eisenhuettenw.* **35** (1964) 1011.
16. H. SCHENCK, E. SCHMIDTMANN and H. MULLER, *ibid.* **31** (1960) 121.
17. J. H. SWISHER, *Trans. TMS-AIME* **242** (1968) 1035.
18. C. WAGNER, *Z. Elektrochem.* **63** (1959) 772.

Received 11 March
and accepted 2 June 1987